Applied Surface Science 354 (2015) 401–407

Contents lists available at ScienceDirect

Applied Surface Science

journal homepage: www.elsevier.com/locate/apsusc

Electronic structure and soft magnetic properties of Se/FeSiAl (110) films

V. Cardoso Schwindt[a], J.S. Ardenghi[a], P. Bechthold[a], A. Juan[a], B. Setina Batic[b], M. Jenko[b,*], E.A. González[a], P.V. Jasen[a]

[a] Departamento de Física, Universidad Nacional del Sur & IFISUR (UNS-CONICET), Av. Alem 1253, (8000) Bahía Blanca, Argentina
[b] Institute of Metals and Technology, Lepi pot 11, 1000 Ljubljana, Slovenia

ARTICLE INFO

Article history:
Received 28 November 2014
Accepted 19 April 2015
Available online 25 April 2015

Keywords:
DO3 structure
DFT
Soft magnetic materials
Surface segregation

ABSTRACT

The Se adsorption at different coverages on DO3 FeSiAl(110) surface is studied using density functional theory (DFT). Se adsorption is favorable in almost all surface high-symmetry sites, except for the bridge site formed by Fe–Si atoms. The most stable is a hollow site formed by four Fe atoms with adsorption energy of −5.30 eV. When the coverages increase, the energies decrease in the case of hollow sites. The surface present a reconstruction after Se adsorption, being the most important at 1/2 ML. The local magnetic moment for Fe atoms increase for the type A (all nearst neighbours (nn) are Fe atoms) and decrease for the type B (nn are Fe, Si and Al atoms). The most affected metal orbitals are Fe 4s and 4p. In the case of the hollow site the surface Fe–Fe bond is weakened after Se adsorption. A Fe–Se bond is developed at all coverages in both sites being the most important on top (d_{Fe-Se} = 2.23 Å, OP: 0.774 at 1/4 ML). The first and second layer Fe–Fe bond increase at 1/4 ML and decrease at 1/2 and 1 ML. Small Se–Se bonding interaction appear at 1/2 ML and increase noticeable for 1 ML. For the top site, the Se–Se bond appears at all coverage. The Fe–Fe surface bonds also decrease its strength with respect to the clean surface at all coverage. The first and second layer Fe–Fe bond increase at all coverage.

1. Introduction

The development of GHz-electromagnetic (EM) wave absorbers is important to solve the induced EM interference (EMI) problem. A number of materials, such as iron, cobalt, nickel, metal alloys and ferrites, are conventionally used as electromagnetic absorbers. However, high specific gravity and high costs limit the applicability of these materials, and there is an increasing interest in microwave absorption materials with a high absorption rate, wide absorption band, thin coating and light weight [1].

With the fast development of wireless communication applications and the widespread use of microwave devices over the 1–4 GHz range, the emerging hazards of microwaves and electrical equipment on human health have attracted the interest of many scientists. Incident microwaves are attenuated due to absorbing/shielding materials and the microwaves reflected become much weaker as compared to the incident waves. At present, the absorbent is the key factor dominating absorbing and shielding properties [2].

FeSiAl alloy as a traditional soft magnetic material applied in EMI area, has attracted much interests due to its excellent magnetic properties, good temperature stability and low cost. However, these materials present some difficulties in increasing the permeability in GHz region due to their low Snoek's limit and can only be used as good microwave absorbers in the low GHz range [2–4].

FeSiAl alloys are also known as silicon steels. This type of steel is tailored to produce certain magnetic properties, such as a small hysteresis loop area and high permeability [5]. Fe_3Si and Fe_3Al alloys have excellent soft magnetic properties and they are used for motor and transformer cores. The relationship between structural and magnetic properties in Fe-based magnetic systems has been extensively studied [6–10]. It is interesting to note that the DO3 ordering is rather easily achieved in the Fe_3Si alloy, whereas it is extremely difficult in the case of Fe_3Al alloy. Ma et al. [11] have assesses intrinsic properties of magnetically ordered $Fe_3Al_{1-x}Si_x$ alloys and the effect of Si substitution for Al the ordered alloys. Dopant elements though added in very small concentrations, have a great effect on the final properties of the steel [5,12].

Sun et al. [13] studied the irregular-shaped FeSiAl powder mixed with graphite. The results demonstrated that the milled FeSiAl/graphite absorbers possess higher permittivity, slightly increased permeability, and better microwave absorption

* Corresponding author. Tel.: +386 1 4701950.
E-mail addresses: monika.jenko@imt.si, monica.jenko@gmail.com (M. Jenko).

http://dx.doi.org/10.1016/j.apsusc.2015.04.122
0169-4332/

properties than those of raw FeSiAl powders in the frequency range of 2–18 GHz. Additionally, the results also indicate that, although the raw FeSiAl powder is a good EM wave absorbers in the low GHz range, the milled flake-shaped FeSiAl/graphite composites exhibit superior microwave absorption performance due to the combination effects of high dielectric loss property of the added graphite and the high planar anisotropy of the flake-shaped particles obtained after the ball-milling.

Han et al. [14] have studied the effect of attrition time on the particle shape and materials properties. They also study the high frequency properties of Fe–Si–Al particles.

It has been shown that a small addition of Se has a beneficial effect on the texture and magnetic properties of the FeSi alloys [15]. Se is a surface-active element that segregates to free surfaces at elevated temperatures (above 850 °C). X-ray photoelectron spectroscopy (XPS) studies show a correlation between Si and Se segregation in the form of co-segregation. No chemical bonding between the two elements has been observed in previous XPS studies [16]. Se also has a crucial effect on surface reconstruction and recrystallization as well as on the grain growth of individual crystal grains in the alloy. Upon surface segregation, roof-top-like morphologies form in the grains with observable amounts of Se segregated species.

Recently, DFT theoretical studies of elements belonging to the same group of Se and other atoms adsorbed on Fe surfaces was published [17–20]. Gonzalez et al. [22] by performing DFT calculations found Se located on a long-bridge site on bcc Fe(110) at low coverage. They also reported that the Se caused an ordered reconstruction and relaxation of the Fe surface. Cardoso Schwindt et al. [23] also studied the effect of Se in the bcc Fe(100) and Fe(111) surfaces. Their calculations predict that it is possible to achieve a decrease of about 50% in the magnetic moment on the Fe(100) surface after Se adsorption. However, the most stable Se adsorption occurs on the Fe(111) surface. Çakmak et al. investigated the adsorption of Se on Si(001) [21].

The aim of the present work is to analyze the adsorption of Se on FeSiAl(110) and to compare with our previous calculations on bcc Fe(110). We also computed changes in surface geometry, magnetic moment, electronic structure, and bonding after Se adsorption.

2. Theory and models

2.1. Computational details

Calculations were performed using the density functional theory (DFT) as implemented in the VASP code [24–26]. Exchange and correlation energies were calculated with the Perdew–Burke–Ernzerhof form of the spin-polarized generalized gradient approximation (GGA-PBE) [27]. Spin-polarization and non-linear core corrections were included in FeSiAl system calculations as to correctly account for its magnetic properties [28]. Spin polarization has been shown to have a major effect on the adsorption energies of magnetic systems and may alter the topology of potential energy surfaces [29]. The electron–ionic core interaction was represented by ultra-soft pseudo-potentials [30]. A plane-wave basis with an energy cutoff of 330 eV was used to expand electronic wave functions. Brillouin zone integrations were performed on a special k-point mesh generated by the Monkhorst–Pack scheme ($12 \times 12 \times 12$ in bulk) [31]. In order to accelerate convergence, the first order Methfessel–Paxton method with a Fermi surface smearing of 0.2 eV was adopted for fractional occupancies [32]. The calculations for the bulk crystal structure give a lattice constant of DO3 FeSiAl equal to 5.750 Å, which is in good agreement with that reported for Legarra et al. [33]. The local spin magnetic moment for a Fe atom is $1.66\mu_B$ (Bohr magnetron), in full agreement with previous calculations [34]. Bader analysis was used to calculate magnetic moments and electronic charges on atoms [35].

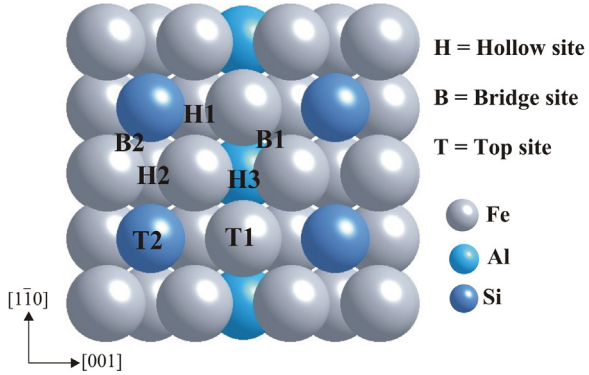

Fig. 1. Schematic top view of (110) surface of the FeSiAl alloy. The high symmetry sites are indicated (find full nomenclature in text).

2.2. Surface models

FeSiAl alloy has DO3-type crystal structure, which is composed of four interpenetrating fcc lattices shifted by 1/4th of the main diagonal [36,37]. In this structure, there are two non-equivalent Fe positions, one surrounded by eight Fe atoms and the other surrounded by four Fe, two Si and two Al atoms denoted as Fe_A and Fe_B respectively.

The considered surface was modeled by a slab consisting of several (up to 15) atomic layers separated by a vacuum layer of 15 Å, and periodically repeated throughout space. We used a *k*-point mesh of $8 \times 8 \times 1$ for the surface, which provided well-converged total energy. The positions of the 15 layer slab were fully optimized until the forces on each atom were less than 0.02 eV/Å. Test calculations for denser *k*-point meshes showed that the uncertainty of surface energies is within 0.01 J/m^2 and that of relaxations is within 0.5%.

In this work, selenium is adsorbed at the high-symmetry surface sites in the (110) plane: two bridge (B1: Fe–Fe atoms; B2: Fe–Si atoms), two top (T1: Fe atom; T2: Si atom), and three fourfold hollow sites (H1: 3Fe–Si; H2: 2Fe–2Si; H3: 4Fe atoms) (see Fig. 1). We also studied different Se coverages (1/4, 1/2, and 1 ML) considering the adsorption only in two stable sites, H and T (see Fig. 2). The adsorption energies were calculated using the following equation:

$$\Delta E_{ads} = \frac{[E_{slab+nSe} - E_{slab} - nE_{Se}]}{n} \quad (1)$$

Here, the first term on the right-hand side is the total energy for the FeSiAl surface supercell plus n Se atoms, depending on the coverage. The second term is the total energy for the FeSiAl supercell; the third term is the Se atom total energy. This last term is calculated by placing a Se atom in a cubic box with 10 Å sides and carrying out a Γ-point calculation.

In order to understand FeSiAl(110)–Se interactions, we used the concepts of density of states (DOS) and crystal orbital overlap population (COOP). The DOS curve is a plot of the number of orbitals as a function of energy. The integral of the DOS curve over an energy interval gives the number of one-electron states in that interval; the integral up to the Fermi level (E_F) gives the total number of occupied molecular orbitals. If the DOS is weighed with the overlap population between two atoms, the COOP is obtained. The integration of the COOP curve up to E_F gives the total overlap population of the specified bond orbital and it is a measure of the bond strength. If an orbital at certain energy is strongly bonding between two atoms, the overlap population is strongly positive and the COOP curve will

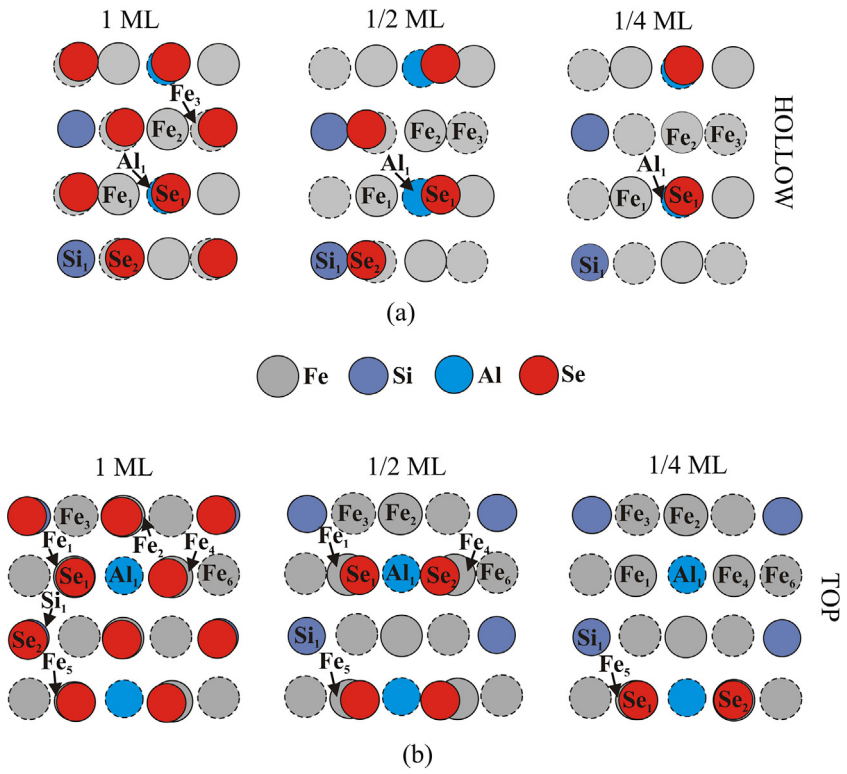

Fig. 2. Schematic top view of the Se/FeSiAl(110) surface at 1/4 ML, 1/2 ML and 1 ML for hollow site (a) and top site (b). The dotted line indicate second layer.

be large and positive around that energy. Similarly, negative COOP around certain energy corresponds to antibonding interactions. The COOP curves were computed using the SIESTA code [38,39].

3. Results and discussion

3.1. Surface geometry and magnetic properties for a clean surface and Se adsorption energy

Let us first considerer the FeSiAl(110) clean surface. Our calculations shown that the computed layer separation between the first and the second layer, Δ_{12}, have different values for the surface atoms. The Fe_A and Si atoms contract (−5% and −3% respectively) while the Fe_B atoms have a small outward relaxation (0.3%). The abrupt termination of surface and the reduced coordination of atoms on the surface lead to an enhancement of local magnetic moment (μ) of the superficial Fe atoms. We found that the Fe_A and Fe_B atoms have a μ of $2.60\mu_B$ and $2.23\mu_B$ respectively. The explanation for this different behaviour in the local magnetic moments of Fe atoms can easily be explained if we consider the local environment of the Fe sites and the relative affinity of Si and Al for Fe. The changes in the magnetic moment can also be explained by comparing the d band of the DOS near the Fermi level for a surface Fe atom (see Fig. 3). Comparing with the local magnetic moment of superficial Fe atoms in the Fe(110) surface ($2.67\mu_B$), we can see that the values for Fe_A atoms are similar while those for Fe_B atoms are lower.

Table 1 presents the adsorption energy of one Se atom on FeSiAl (110) surface, the smallest Fe–Se and Si–Se distances, and the height of Se atom over the surface for different adsorption sites. The Se adsorption on the FeSiAl(110) surface is energetically favorable at a low coverage except for the B1 site (see Table 1). The most stable site is the four-fold hollow H3 with an energy value of −5.30 eV (see Fig. 1 for geometry). The computed Fe–Se distances are between 2.209 and 2.581 Å, while Si–Se distances are between 2.253 and 3.968 Å. Se atoms are located between 1.675 and 2.253 Å above the surfaces. Similar Fe–Se and height distances were determined for Se on the bcc Fe(110), Fe(100) and Fe(111) surfaces [22,23]. Unfortunately, there are no experimental data available for a direct comparison for Se adsorption in this alloy.

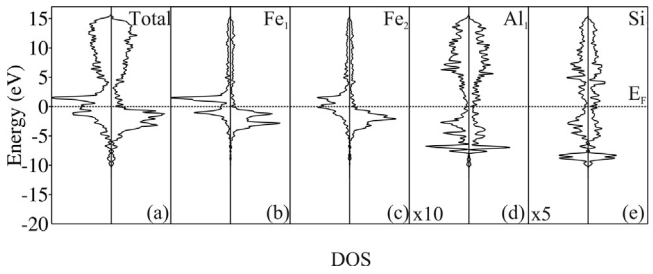

Fig. 3. DOS curves for FeSiAl(110) clean surface: total (a), projected DOS for a Fe_1 atom (b), for a Fe_2 atom (c), for a Al atom (d) and for a Si atom (e).

As mentioned before, the Se adsorption on the B1 bridge site is not stable. Thus, there are two possible ways to generate coverage. They can be achieved by covering the hollow sites or the top sites of the surface with Se adatoms.

When considering the overlap population (OP) after geometry relaxation, the highest metal–metal OP is the Fe–Si followed by the Fe–Al. The Fe_1–non-ferrum bonds have a higher OP than the

Table 1
Adsorption energy of one Se atom on FeSiAl(110) surface, smallest Fe–Se (d_{Fe-Se}) and Si–Se (d_{Si-Se}) distances, and height of the Se atom over the surface (h) for the different adsorption sites.

Site	B1	B2	T1	T2	H1	H2	H3
E_{ad} (eV)	Unstable	−3.96	−3.72	−3.22	−4.53	−3.95	−5.30
d_{Fe-Se} (Å)	–	2.318	2.209	–	2.344	2.342	2.581
d_{Si-Se} (Å)	–	2.371	–	2.253	2.505	2.897	3.968
h (Å)	–	1.827	2.209	2.253	1.703	1.905	1.675

Table 2
Electron orbital occupation, overlap population (OP), ΔOP%, and distances for FeSiAl(110) before and after Se adsorption on hollow site.

Structure	Electron orbital occupation			Bond type	OP	ΔOP%[†]	Distance (Å)
	s	p	d				
Clean surface							
Fe_1	0.60	0.37	7.59	Fe_1–Fe_2	0.285		2.539
Fe_3	0.55	0.24	6.54	Fe_1–Fe_3	0.067		2.879
Si	1.44	2.02	0.00	Fe_1–Si	0.394		2.447
Al	1.17	1.30	0.00	Fe_1–Al	0.263		2.539
				Fe_3–Si	0.295		2.428
				Fe_3–Al	0.232		2.490
Surface + Se (1/4 ML)[a]							
Fe_1	0.55	0.44	6.89	Fe_1–Fe_2	0.174	−38.9	2.583
Fe_3	0.56	0.24	6.63	Fe_1–Fe_3	0.081	+20.5	2.871
Si	1.17	1.31	0.00	Fe_1–Si	0.395	+0.2	2.406
Al	1.43	1.96	0.00	Fe_1–Al	0.241	−8.5	2.573
Se	1.75	4.23	0.06	Fe_1–Se_1	0.554	–	2.332
				Si–Se_1	0.001	–	3.962
				Al–Se_1	0.009	–	3.723
				Fe_3–Si	0.303	+2.7	2.388
				Fe_3–Al	0.246	+5.9	2.490
Surface + Se (1/2 ML)[a]							
Fe_1	0.49	0.35	6.83	Fe_1–Fe_2	0.148	−48.0	2.552
Fe_3	0.56	0.27	6.79	Fe_1–Fe_3	0.066	−2.2	3.050
Si	1.18	1.32	0.00	Fe_1–Si	0.198	−49.9	2.535
Al	1.35	1.84	0.00	Fe_1–Al	0.217	−17.5	2.714
Se	1.77	4.18	0.06	Fe_1–Se_1	0.353	–	2.486
				Si–Se_1	0.604	–	2.317
				Al–Se_1	0.002	–	3.862
				Fe_3–Si	0.336	+14.0	2.341
				Fe_3–Al	0.257	+11.0	2.490
				Se_1–Se_2	0.006	–	3.071
Surface + Se (1 ML)[a]							
Fe_1	0.51	0.30	6.87	Fe_1–Fe_2	0.134	−52.8	2.576
Fe_3	0.55	0.25	6.75	Fe_1–Fe_3	0.061	−9.4	2.942
Si	1.17	1.31	0.00	Fe_1–Si	0.287	−27.1	2.449
Al	1.39	1.70	0.00	Fe_1–Al	0.219	−16.8	2.649
Se	1.75	3.14	0.18	Fe_1–Se_1	0.394	–	2.412
				Fe_1–Se_2	0.038	–	2.953
				Si–Se_1	0.142	–	2.945
				Al–Se_1	0.002	–	3.970
				Fe_3–Si	0.361	+22.4	2.412
				Fe_3–Al	0.244	+5.3	2.490
				Se_1–Se_2	0.258	–	2.509

[†] The percentage of change is with respect to the clean surface.
[a] The geometry is shown in Fig. 2.

Fe_3–non-ferrum (25% for Si and ~12% for Al atoms respectively) (see Table 2). The Fe–Fe bond from atoms of the surface present lower OP than that on Fe(110) (−24.6%) but the Fe–Fe bond, with one them in the second layer, have a more pronounced difference (−65.7%) for very similar distances (2.48 and 2.86 Å in bcc Fe vs. 2.539 and 2.879 Å in the alloy, respectively).

Regarding the chemical bonding analysis, the COOP curves show several small hybridization peaks in the region of (−10, −5) eV for Fe–Fe bonds and an anti-bonding peak on the Fermi level (see Fig. 4a). The COOP curves for the Fe–Al and Fe–Si bonds are all bonding (see Figs. 4b and c).

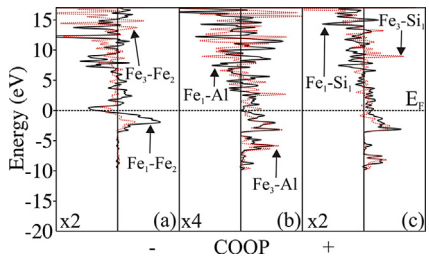

Fig. 4. COOP curves for FeSiAl(110) clean surface: Fe–Fe (a), Fe–Al (b) and Fe–Si (c) bond.

3.2. Surface geometry and magnetic properties after Se coverage

When considering Se coverage in the hollow site, the layer separation between the first and the second layer, Δ_{12}, contracts for about −0.6% and −6.2% for Fe_A and Si atoms respectively, while Fe_B atoms have a small outward relaxation of 0.4% in the case of 1/4 ML coverage. The most important reconstruction of the surface occurs at 1/2 ML coverage, where some Fe_B and Si atoms contract (−6.5% and −11.6% respectively) whereas the Fe_A and some Fe_B atoms have an outward relaxation of 3.8% and 11.6% respectively (see Fig. 2). For a 1 ML coverage the Fe_A and Si atoms contract for −6.1% and −15.7% respectively, while the Fe_B atoms have an outward relaxation of 5.1%. On the other hand, when considering the coverage on the top site, for the 1/4 and 1/2 ML almost all the surface atoms contractions are more noticeable at the 1/2 ML coverage. For the 1 ML case, all the surface atoms contract.

In the case of Se coverage in a hollow site, the Fe_A atoms have a magnetic moment, which is slightly higher compared to the values of the clean surface whereas the Fe_B has lower magnetic moments. The behaviour in the magnetic moment of Fe atoms is consequent with the increase of the spin up contribution in PDOS for Fe_1 (type A) near the Fermi level (see Fig. 5b, h and c), and with the decrease in the spin up contribution to PDOS of Fe_2 atom (type B) near E_F (see Fig. 5c, i and o). The PDOS curves for Al and Si atoms show a slight

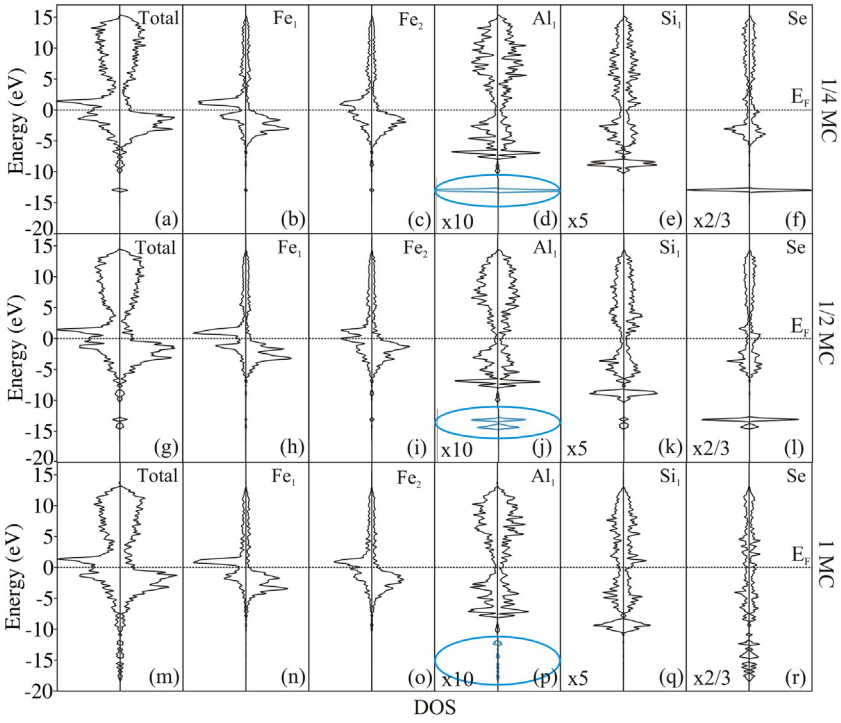

Fig. 5. DOS curves for the Se/FeSiAl(110) system in hollow site: Total (a), (g), and (m); projected DOS for a Fe_1 atom (b), (h), and (n); projected DOS for a Fe_2 atom (c), (i), and (o); projected DOS for a Al_1 atom (d), (j), and (p); projected DOS for a Si_1 atom (e), (k) and (q); and projected DOS for a Se atom (f), (l), and (r). The ellipse stamp/mark indicated a zoomed area times 100.

spin polarization (see Fig. 5). The lower magnetic moments are obtained for the 1/2 ML coverage (1.69μ_B). This can be explained considering a noticeable rearrangement in the surface. At the top site coverage, the magnetic moments of Fe_A atoms for 1/4 and 1/2 ML coverages are higher than those corresponding to the clean surface. In the case of 1ML the magnetic moments of the Fe atoms are lower. The magnetic moments for the Fe_B atoms are lower than on the clean surfaces, but the values increase slightly with the coverage, and the lowest value is 1.43μ_B at 1/2 ML.

The adsorption energy decreases from −5.28 eV (1/4 ML) to −2.20 eV (1 ML) at hollow site coverage. This is because Se–Se interaction is possible at 1 ML and not possible at 1/4 ML. On the other hand, in the case of top site the stable configurations are for 1/2 and 1 ML with adsorption energies of −3.66 eV and −3.50 eV respectively.

DOS analysis, before and after Se adsorption at hollow site for different coverages on FeSiAl(110), gives an indication of adsorbate–substrate interaction (see Figs. 3 and 4). As in our previous study for Se/Fe(110), we detected that the most affected metal orbitals are Fe 4s and 4p [22]. The projection of Se 4p orbitals presents a contribution in the Fe d band region with a broadening for all coverages (compare Fig. 3a and b with Fig. 5a and b). For 1/4 ML the Se 4s orbital presents a sharp peak at −13.1 eV below E_F, this peak is 1.8 eV more stabilized than the one corresponding to Fe(110). When the coverage increases to 1/2 ML the peak decreases in intensity and splits. For 1 ML the Se 4s and 4p bands show a strong hybridization with Se 4p band extending from E_F to −10 eV and Se 4s band extending from −11.5 eV to −18.8 eV (see Fig. 5f, l and r). That sharp peak also appears in the Fe projections and shows the same behaviour that in the case of Se projection when the coverage increases (see Fig. 5 for Fe_1 and Fe_2 projections). The Al DOS projection show a little peak at −13.1 eV due to the interaction with Se 4p orbital for the 1/4 ML, that splits and decreases in intensity for 1/2 ML and 1 ML (see Fig. 5d, j and p). In the case of Si atom, the peak is small at 1/4 ML, splits to an increase in intensity at 1/2 ML coverage, while in the case of 1 ML it splits in several peaks and considerably decreases in intensity (see Fig. 5e, k and q). This behaviour is due to Se–Se interaction that shows up since 1/2 ML. At the top coverage the hybridization starts at 1/4 ML, due to the Se–Se interaction. In this case, the Al atoms are not affected after Se adsorption (see Fig. 7).

Regarding changes in the chemical bonding, after Se adsorption the COOP curves for Fe–Fe bond show a small decrease in the area between −5 eV and E_F, which is an indicative of a bond weakening (compare Fig. 6a, g and m with Fig. 4a). Also, a small peak at −13 eV develops for 1/4 and 1/2 ML while for 1ML, a small hybridization can be observed from −17 to −7 eV. The Fe–Al bond shows almost no changes except for a small peak at −13 eV that vanishes when the coverage increases (see Figs. 4b and 6b, h and n). Fe_1–Si bond do not show significant changes after Se adsorption. In the case of Fe_3–Si at 1/2 ML coverage several peaks appear in the region (−14, −13) eV. At 1/4 ML an important Fe–Se interaction develops at −3.0 and −13.0 eV (see Fig. 6d). At 1/2 and 1 ML the Fe–Se peaks decrease in intensity and are broadened in the region of (−15, −14) eV and (−4 eV, E_F) for the 1/2 ML and (−17, −14) eV and (−5, E_F) for the 1 ML (compare Fig. 6d with Fig. 6j and p respectively).

In the cases of the Al–Se COOP curves, a peak at −13 eV is observed for 1/4 ML coverage that splits and diminishes in intensity at 1/2 and 1 ML (see Fig. 6e, k and q). Also, several peaks can be observed in the region from −5 eV to E_F that shows a decrease of intensity when the coverage increases.

In the case of Si–Se bond, at 1/4 ML there are two peaks at (−5 eV, E_F), one bonding and another antibonding that became all bonding for 1/2 ML and 1 ML. At 1/2 ML several bonding peak appear in the region (−14, −13) eV while at 1 ML there is broadening and an increase of the s and p orbitals in the region (−17, −7) eV. The Se–Se bond is only formed at 1 ML and its COOP curve presents hybridization at (−17, −10) eV and (−4, E_F) eV.

The Fe_1–Fe_2 bonds are most affected after Se adsorption and the bond weakening increases with the coverage (−38.9% at 1/4 ML, −48.0% at 1/2 ML and −52.8% at 1 ML) (see Table 2). However, the Fe_3–Fe_1 OP shows an increase at 1/4 ML (+20.5%) and a decrease at

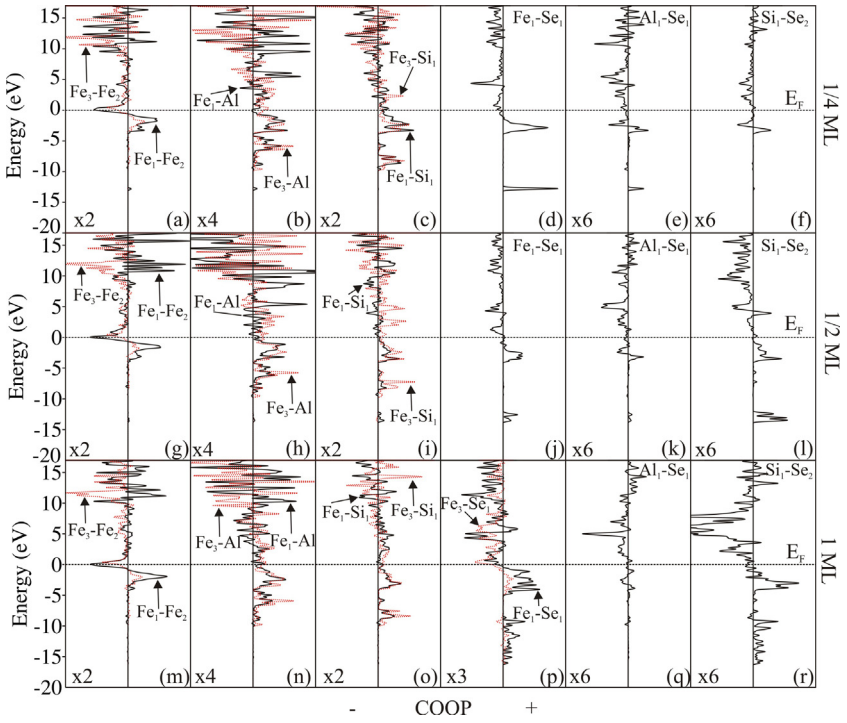

Fig. 6. COOP curves for the Se/FeSiAl(110) system in hollow site: Fe–Fe (a), (g) and (m); Fe–Al (b), (h) and (n); Fe–Si (c), (i) and (o); Fe–Se (d), (j) and (p); Al–Se (e), (k) and (q); Si–Se (f), (l) and (r) bonds.

1/2 and 1 ML (−2.2 and −9.4% respectively). This behaviour can be explained considering the surface reconstruction at different coverages. The Fe_3–Al and Fe_3–Si OP bonds show an increase after Se adsorption. The Fe_1–Si OP bonds decrease at 1/2 and 1 ML, and a small increase at 1/4 ML is observed (+2.7%). The Fe_1–Al OP bonds are weakened after Se adsorption (see Table 2).

Si–Se and a small Al–Se OP bonds are detected at all coverages. The most important Si–Se OP value is at 1/2 ML for the hollow site (OP: 0.604; d_{Si-Se} = 2.317 Å) A Fe–Se bond is developed at all coverages in top sites being the most important at 1/4 ML (d_{Fe-Se} = 2.23 Å, OP: 0.774). In the case of hollow site, the Fe–Se OP bonds present similar values for 1/2 and 1 ML, where a second Fe–Se interaction is

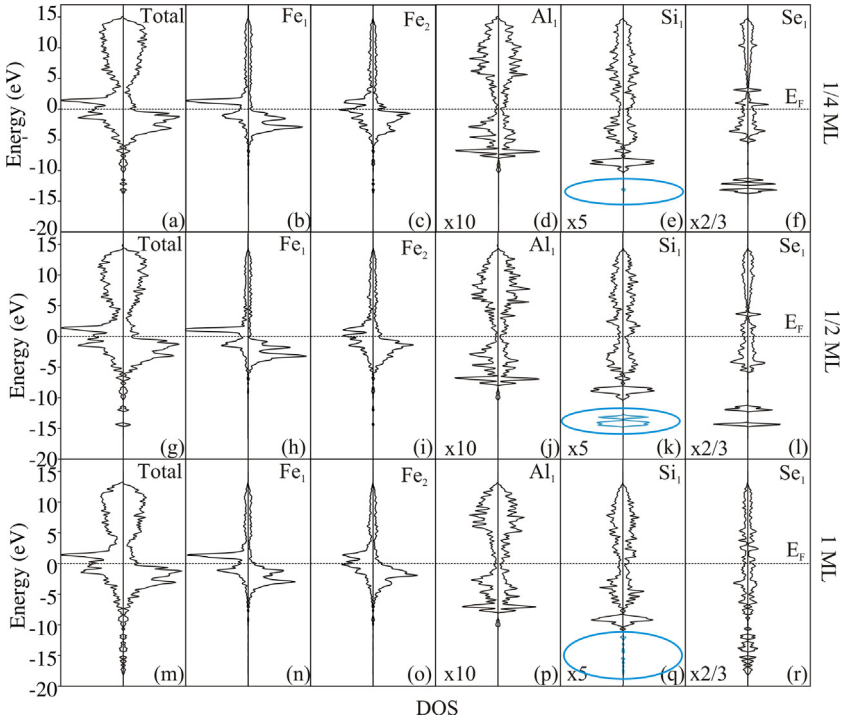

Fig. 7. DOS curves for the Se/FeSiAl(110) system in hollow site: Total (a), (g), and (m); projected DOS for a Fe_1 atom (b), (h), and (n); projected DOS for a Fe_2 atom (c), (i), and (o); projected DOS for a Al_1 atom (d), (j), and (p); projected DOS for a Si_1 atom (e), (k) and (q); and projected DOS for a Se atom (f), (l), and (r). The ellipse stamp/mark indicated a zoomed area times 100.

detected. Nevertheless, the most important Fe–Se bond OP is found at 1/4 ML (0.554) (see Table 2).

If we compare both coverage sites (hollow and top), the Fe_1–Fe_2 bonds in the top site are weakened but not in line with the increase of Se coverage at the surface, which is the case in the hollow sites. The most important weakening is found at the 1/2 ML coverage (−30%), followed by 1ML and in the case of 1/4 ML it amounts to only 6%. On the other hand, the Fe_1–Fe_3 bonds OP increase at all coverages, the most important being at 1/2 ML with 37.7%. This can be explained considering a great reconstruction that is observed in the surface after Se coverage. The Fe_4–Fe_6 bonds increase at 1/4 and 1/2 ML but are weakened at 1ML. The Fe–Si and Fe–Al behaviors are more random than in the hollow case. The main difference between both considered cases are that at the top site a Se–Se bond is detected at all coverages, the most important one is observed at 1/2 ML.

4. Conclusions

By using periodic DFT calculations we found that the most stable Se adsorption site is a tetra coordinate hollow location formed by Fe atoms. At the hollow site case the adsorption energies decrease from −5.28 eV to −2.20 eV when the coverages increase from 1/4 ML to 1 ML. The coverage on top site shows no trend is found, being the most stable energy at 1/4 ML. The surface suffers and important reconstruction at 1/2 ML for both considered cases. The local magnetic moment increase for the Fe_A and decrease for Fe_B. The most important reduction on the local magnetic moment of Fe_B atoms is obtained at 1/2 ML. The mean magnetic moment decrease because the alloy is mainly compound by Fe_B atoms. This alloy has a stable ferromagnetism and interesting magnetic properties that are improved by the Se adsorption. The DOS plots indicate a strong hybridization for Se projection at 1ML and also in the Fe, Al and Si nn projections. The Fe–Fe surface bond OP decrease at all coverage for both cases. The first and second layer Fe–Fe bond increase for 1/4 ML and decrease for 1/2 and 1 ML in the case of hollow site, while for the top site increase at all coverage. The Fe–Se bonds are developed for the both site at all coverage, being the most important OP value 0.774 at 1/4 ML for the top site. In the case of hollow site at 1/2 ML a strong Si–Se bonding interaction is present. A Se–Se bond is present at all coverages for the top site. In the case of the hollow site there is a small Se–Se interaction at 1/2 ML (0.006) and increase noticeable at 1 ML (0.258).

Acknowledgements

Our work was supported by SGCyT-UNS and PICT 2186, Grant MHES-MINCyT SLO/11/07 and CIC Buenos Aires Province. A Juan, E. A. Gonzalez, P. V. Jasen, and J. S. Ardenghi are members of CONICET. P. Bechthold is a CONICET fellow. It was supported also by the project P2-0132 Surface Physics and Chemistry of metallic materials (M. Jenko), of Slovenian Research Agency-ARRS.

References

[1] W. Yang, Y. Fu, A. Xia, K. Zhang, Z. Wu, J. Alloys Compd. 518 (2012) 6–10.
[2] W. Zhang, Y. Xu, L. Yuan, J. Cai, D. Zhang, J. Mater. Sci. Technol. 28 (2012) 913–919.
[3] T.D. Zhou, P.H. Zhou, D.F. Liang, L.J. Deng, J. Alloys Compd. 484 (2009) 545–549.
[4] A.H. Kasama, C. Bolfarini, C.S. Kiminami, W.J. Botta Filho, Mater. Sci. Eng. A 449 (2007) 375–377.
[5] B.S. Batic, M. Jenko, J. Vac. Sci. Technol. A 28 (2010) 741–744.
[6] J. Moss, P. Brown, J. Phys. F: Met. Phys. 2 (1972) 358.
[7] G.A. Pérez Alcázar, E. Galvão da Silva, J. Phys. F: Met. Phys. 17 (1987) 2323.
[8] G.A. Pérez Alcázar, E. Zamora Ligia, J.D. Betancur-Ríos, J.A. Tabares, J.M. Greneche, J.M. González, Phys. B 384 (2006) 313.
[9] B. Sprusil, B. Chalupa, Intermetallics 7 (1999) 635.
[10] V. Sebastian, N. Lakshmi, K. Venugopalan, Intermetallics 15 (2007) 1006.
[11] X.G. Ma, J.J. Jiang, S.W. Bie, L. Miao, C.K. Zhang, Z.Y. Wang, Intermetallics 18 (2010) 2399–2403.
[12] D.S. Petrovic, M. Jenko, M. Jeram, F. Marinšek, V. Prešern, Strojarstvo 48 (2006) 45.
[13] J. Sun, H. Xu, Y. Shen, H. Bi, W. Liang, R.-B. Yang, J. Alloys Compd. 548 (2013) 18.
[14] M. Han, D. Liang, J. Xie, L. Deng, J. Appl. Phys. 111 (2012) 07A317.
[15] M. Jenko, M. Godec, H. Viefhaus, H.J. Grabke, Mater. Sci. Forum 294–296 (1998) 747.
[16] M. Jenko, J. Fine, D. Mandrino, Surf. Int. Anal. 30 (2000) 350.
[17] S.R. Chubb, W.E. Pickett, Phys. Rev. B 38 (1988) 10227.
[18] R. Wu, A.J. Freeman, G.B. Olson, Phys. Rev. B 47 (1993) 6855.
[19] S. Pick, P. Legare, C. Demangeat, Phys. Rev. B 75 (2007) 195446.
[20] P. Błoński, A. Kiejna, J. Hafner, Surf. Sci. 590 (2005) 88.
[21] M. Çakmak, G.P. Srivastava, Ş. Ellialtıoğlu, K. Çolakoğlu, Surf. Sci. 507–510 (2002) 29.
[22] E.A. González, P.V. Jasen, M. Sandoval, P. Bechthold, A. Juan, B.S. Batic, M. Jenko, Appl. Surf. Sci. 257 (2011) 6878.
[23] V. Cardoso Schwindt, J.S. Ardenghi, P. Bechthold, E.A. González, P.V. Jasen, A. Juan, B.S. Batic, M. Jenko, Appl. Surf. Sci. 315 (2014) 252–260.
[24] G. Kresse, J. Hafner, Phys. Rev. B 47 (1993) 558.
[25] G. Kresse, J. Furthmüller, Phys. Rev. B 54 (1996) 11169.
[26] G. Kresse, J. Furthmüller, Comput. Mater. Sci. 6 (1996) 15.
[27] J. Perdew, J.A. Chevary, S.H. Vosko, K.A. Jackson, M.R. Pederson, D.J. Singh, C. Fiolhais, Phys. Rev. B 46 (1992) 6671.
[28] S.G. Louie, S. Froyen, M.L. Cohen, Phys. Rev. B 26 (1982) 1738.
[29] Q. Ge, S.S. Jenkins, D.A. King, Chem. Phys. Lett. 327 (2000) 125.
[30] D. Vanderbilt, Phys. Rev. B 41 (1990) 7892.
[31] H.J. Monkhorst, J.D. Pack, Phys. Rev. B 13 (1976) 5188.
[32] M. Methfessel, A.T. Paxton, Phys. Rev. B 40 (1989) 3616.
[33] E. Legarra, E. Apiñaniz, F. Plazaola, J.A. Jimenez, A.R. Pierna, J. Mag. Mag. Mater. 320 (2008) e688–e691.
[34] T.D. Zhou, L.J. Deng, D.F. Liang, Acta Metall. Sin. (Engl. Lett.) 21 (2008) 191–196.
[35] R.F.W. Bader, Atoms in Molecules – A Quantum Theory, Oxford University Press, Oxford, 1990.
[36] X.G. Ma, J.J. Jiang, S.W. Bie, L. Miao, C.K. Zhang, Z.Y. Wang, Intermetallics 18 (2010) 2399–2403.
[37] T.D. Zhou, L.J. Deng, D.F. Liang, Acta Metall. Sin. (Engl. Lett.) 21 (2008) 191–196.
[38] P. Ordejón, E. Artacho, J.M. Soler, Phys. Rev. B 53 (1996) R10441–R10444.
[39] J.M. Soler, E. Artacho, J.D. Gale, A. Garcia, J. Junquera, P. Ordejón, D. Sanchez-Portal, J. Phys. Condens. Matter. 14 (2002) 2745.